Influence of implant base material on secondary bone healing: an *in silico* study

Gargi Shankar Nayak, Michael Roland, Björn Wiese, Norbert Hort & Stefan Diebels

Taylor & Francis
Taylor & Francis Group

Influence of implant base material on secondary bone healing: an *in silico* study

Gargi Shankar Nayak[a], Michael Roland[a], Björn Wiese[b], Norbert Hort[b,c] and Stefan Diebels[a]

[a]Chair of Applied Mechanics, Saarland University, Saarbrücken, Germany; [b]Institute of Metallic Biomaterials, Geesthacht, Germany; [c]Leuphana University Lüneburg, Institute of Product and Process Innovation, Lüneburg, Germany

ABSTRACT

The implant material at the fracture site influences fracture healing not only from biological perspective but also from mechanical perspective. Biodegradable implants such as magnesium (Mg) based alloys have shown faster secondary bone healing properties as compared to bioinert implants such as titanium (Ti). The general reasoning behind this is the benefit of Mg from biocompatibility perspectives. We studied the effect of Ti and Mg as base materials for implants from mechanical perspectives, where we focused on the displacements at the fracture site of the tibia and their influence on the stimulus for bone healing. We found out that in comparison to Ti, Mg implants have minimal *stress shielding* problem, only which led to better mechanical stimulus at the fracture site.

1. Introduction

The research work to repair bone fracture has improved tremendously in the past years. Where, in the past only bioinert implants such as stainless steel (SLS) (De Fátima Ferreira Mariotto et al. 2011; Goharian and Abdullah 2017) and Ti (McCracken 1999; Rack and Qazi 2006) were applied for fracture healing, nowadays biodegradable implants such as Mg (Razavi et al. 2010; Han et al. 2015) and zinc (Zn) (Farabi et al. 2021) are developing to replace/support them at a fast pace. Biodegradable implants have the advantage over bioinert implants in that they dissolve in the body over time during fracture healing (Ridzwan et al. 2007). Moreover, their low Young's modulus (*E*) also minimizes the *stress shielding* problem, generally seen with Ti and SLS implants, given their *E* value is significantly higher than that of bone (Ridzwan et al. 2007).

In various references, the superior behaviour of Mg implants over inert metallic implants were observed on the basis of their better biological properties to enhance bone regeneration (López et al. 2006; Li and Zheng 2013; Jähn et al. 2016). In the study performed by Jähn et al. the *in vivo* behaviour of Mg-2Ag and SLS intramedullary nails on long bone fracture repair of mice was studied (Jähn et al. 2016). Mg-2Ag nails stimulated a faster bone formation as compared to SS

nails, along with an augmented callus formation, which is necessary for a better secondary bone healing (Bigham-Sadegh and Oryan 2015). In another study, Acar et al. (2020) compared the clinical outcome of application of Mg and Ti screws for biplane chevron medical malleolar osteotomy on patients. Interestingly, both the screws provided similar success. Moreover, as Mg screws degrade during the process, no implant removal operation is needed after the procedure, which is generally the case for Ti implants. However, the mechanical aspects of Mg implants for bone healing are not typically considered in these studies. Moreover, medical experts often want the strength of developed implants to be similar to established implant materials such as SLS and Ti. As the strength of Mg is much lower compared to these established implants, it is also necessary to verify the suitability of Mg as an implant only on the basis of its mechanical stability.

The interfragmentary movement (IFM) at the fracture site provides the critical mechanical stimulus needed for secondary fracture healing (Steiner et al. 2013). There are several models that have been developed to understand its influence on fracture healing (Weinans et al. 1992; Shefelbine et al. 2005; Mehboob and Chang 2014; Miramini et al. 2016; Lu and Lekszycki 2017; Mehboob and Chang 2018; Ganadhiepan et al. 2021). Claes and Heigele (1999)

have developed one of the most known tissue differentiation theory models which undertakes the influence of local stress and strain conditions in the callus due to IFM on its secondary healing regime. The secondary fracture healing in this approach takes two strains due to IFM into account: octahedral shear strain that relates to the shape change in the callus and volumetric strain that relates to volume change in the callus. This model was further modified by Shefelbine et al. (2005) for development of a fuzzy logic to describe the conditions for secondary bone healing. The interplay between these two strains determines the differentiation of mesenchymal cells into different categories. This theory has been used successfully in various simulation studies to predict the best conditions for fracture healing (Shefelbine et al. 2005; Braun et al. 2021; Orth et al. 2023).

Thus, in this research work, this previous knowledge was used to develop a computational framework to visualize the difference in the mechanical stimulus, based on the selection of implant base material. The implant placed at the tibia fracture site was chosen as base material: a. Mg alloy (AZ91) and b. Ti alloy (Ti6Al4V), and the mechanical conditions of the implant and respective fracture site were measured. This research work is a computational approach to understand the mechanical conditions, excluding the other (biological, chemical) ones to understand the influence of this aspect on fracture healing for the short term. According to the authors' knowledge, this is the first paper that clarifies if a Ti alloy implant can be replaced 1-to-1 by Mg alloy and if the mechanical stability of Mg alloy is sufficient for fracture stabilization and for bone healing.

2. Materials and methods

2.1. Implant design

The implant strategy chosen for the simulation is shown in Figure 1. The implant depicted comes from an in-house generated computer-aided design (CAD) dataset, based on a standard titanium locking compression plate (LCP) with ten holes and a length of 186 mm. The bone model is generated from a computed tomography (CT) scan of a human cadaveric specimen of a lower leg. The data set originates from the completed BMBF (German Federal Ministry of Education and Research) funded project 'IIP-Extrem' (FKZ: 13GW0124). The donor was a female at the age of 74 with a body height of 152.4 cm (60 in.) and a body weight of 81.65 kg (180 lbs.) with no bone diseases. The CT scan was performed with a Siemens

SOMATOM Definition Edge with a resolution of 0.541 mm as pixel spacing and 0.60 mm distance between two images. To guarantee a good representation of the local bone properties in the simulation models, a six-rod bone density calibration phantom (QRM-BDC/6, QRM GmbH Moehrendorf, Germany) was used during the CT scan.

The segmentation of the tibia and the calibration phantom in the image stack were performed in the image processing and model generation software ScanIP (Synopsys, Mountain View, CA, United States). The images were segmented into different masks (bone, single rods, etc.) with an adaptive threshold procedure, supplemented by a morphological close filter with isotropic values and a mask smoothing with a recursive Gaussian filter with anisotropic values resulting in a high segmentation quality without detectable problems. After segmentation step, a high-resolution adaptive mesh was created from the individual masks in ScanIP. A quadratic tetrahedral mesh of type C3D10 (ten-node tetrahedral element with four integration points) was chosen for simulation studies. The mesh in the callus and fracture site had an edge length of 0.6 mm with 327,176 and 40,723 elements, respectively.

Based on the calibration phantom, a linear regression was used to calibrate the grayscale values given in Hounsfield units (HU) of the CT image stack and to compute the corresponding equivalent mineral density in each voxel of the bone mask. The calibrated equivalent mineral density values are then used to calculate the ash density values with the mapping given in Shefelbine et al. (2005) and the corresponding apparent density values with the equation from Claes and Heigele (1999). In a subsequent step, the local bone properties were used to compute the local material parameters, i.e. E value and Poisson's ratio (v) with the power law relationship from Rho et al. (1995). All the material properties were passed to the FE mesh and stored in the elements of the corresponding masks. The apparent Young's modulus of bone ranged from 0.1 to 22 GPa based on the (trabecular or cortical) region of the bone.

The fracture was generated *via* an image processing step in the ScanIP environment with a Boolean operation between different masks. As fracture, a simple oblique fracture in the diaphyseal segment at an angle of 30° to the tibial axis according to the international classification of the orthopaedic trauma association with AO/OTA 42A2 was chosen. As this computer model is based on a body donation and not based on a real clinical patient, the callus surrounding the
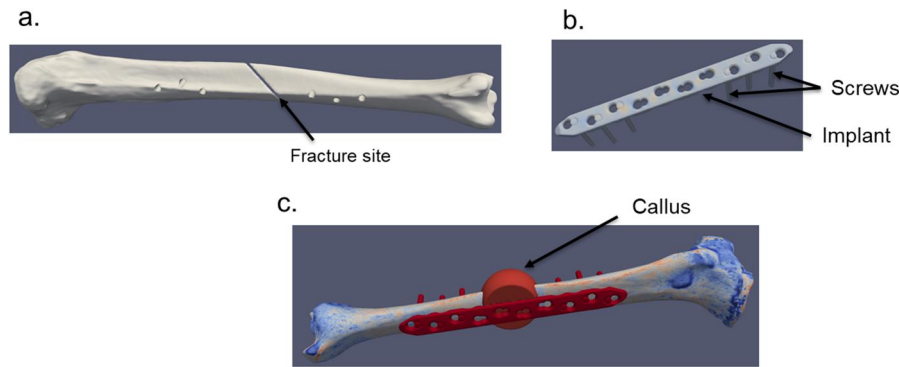
Figure 1. a. The fracture site, b. The implant with screws, and c. the implant fracture assembly with virtual callus for the simulation.

Table 1. The material parameters taken for modelling of implant (Sorriento et al. 2021; Zeng et al. 2022) and callus (Bergmann et al. 2014).

Parameters	Ti (Ti6Al4V)	Mg (AZ91)	Callus
Young's modulus (GPa)	108	45	0.003
Poisson's ratio	0.36	0.28	0.40

fracture also had to be generated virtually. For this purpose, a spherical shape was selected, which is generally chosen in the literature for such simplified models (Lacroix et al. 2002; Schwarzenberg et al. 2021).

The material properties chosen for the implant are shown in Table 1. As the initial stages of bone healing was modelled, the callus properties were taken according to such conditions (soft tissue).

2.2 Simulation methodology

A linear elastic material model was used for simulation. The screws are approximated as cylinders in the simulation model so that no thread pitches need to be simulated. In the case of real patient data-based models, which are segmented from CT data, no thread can be represented due to the resolution of clinical imaging and screws are generally assumed to be cylinders (Braun et al. 2021; Orth et al. 2023). In addition, the model depicts locking screws as they are used in clinical practice, and these are well represented by cylinders with fixed boundary conditions (no friction and no contact). For the connection between bone and implant or screws, a fixed connection was also selected and contact, and friction were avoided. If such aspects are also to be mapped in the simulation, the problem usually arises of making assumptions for unknown parameters.

The simulation of the gait cycle was performed. The knee joint force data regarding the gait cycle was taken from (Bergmann et al. 2014). As in the initial

stages after operation, the legs can sustain only up to 30% of the body weight (Sorriento et al. 2021), the force was adjusted according to these situations. The resulting gait data used for simulation can be seen in Figure 2a. The boundary conditions and the loading locations were derived from the actual movement of Tibia during walking, based on the data from musculoskeletal simulation software AnyBody (AnyBody Technology A/S, Aalborg, Denmark). The simulation was performed in Abaqus/Explicit 2023 with the model from Figure 2b. The Abaqus® simulations were run on the Windows system, with i9 processor (3.50 GHz) and 64 GB RAM. Each simulation took approx. 36 hrs. to finish.

The fuzzy logic approach based on the tissue differentiation theory (Shefelbine et al. 2005) was applied to determine the mechanical stimulus in the callus. The conditions for the tissue differentiation can be seen in Table 2. All the strain conditions that led to bone, cartilage, or connective tissue growth was taken as 'perfect' mechanical stimulus, whereas strain conditions for bone resorption was taken as 'lazy' and the tissue destruction strain conditions was taken as 'too much' as mechanical stimulus.

The strain tensor was measured for each element in the callus and the octahedral shear strain and hydrostatic strain were calculated using a MATLAB code and evaluated according to the limits specified in the literatures (Claes and Heigele 1999; Shefelbine et al. 2005) in Paraview. Moreover, the von Mises stress distribution in the implant was measured to compare the stress shielding tendency of these implants.

3. Results

The von Mises stress distribution in Mg and Ti implants has been shown in Figure 3a,b. In Figure 3c, the overall stress distribution comparison during a gait cycle for both implants were illustrated. Ti implants
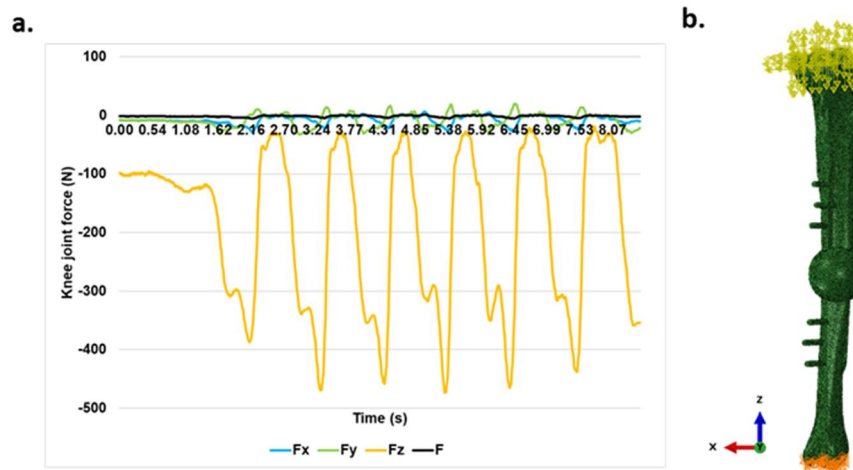
Figure 2. a. The gait cycle used in simulation; b. the direction of forces applied on the model, e.g. Fx corresponds to the force applied on the bone from *x* direction.

Table 2. The strain conditions for determining the mechanical stimulus for secondary healing in callus.

Hydrostatic strain	Octahedral shear strain	Mechanical stimulus
> −0.0001 ≤0.0001	≤0.0001	Lazy
> −0.01 to ≤ −0.0001 >0.0001 to ≤0.06	>0.0001 to ≤0.15	Perfect
rest	Rest	Too much

took higher amount of load than that of Mg. Afterwards, to have a better understanding of the stress conditions at the screw locations under load, the von Mises stress distribution at the screws were visualized for both implants at the same stage of gait cycle in Figure 4. Slightly higher stress was found for Ti-based screws than that of Mg. Moreover, the interfragmentary strain distribution central callus, i.e. the callus that occupies the exact volume of the fracture gap was also measured as can be seen in Figure 5. The octahedral shear strain and hydrostatic strain distribution were measured for both of the implant cases. It was found out that Mg played a lower role in load bearing, as compared to that of Ti. The IFM was found to be higher at the fracture site when Mg implants were used, which led to their higher octahedral shear strain and hydrostatic strain values as compared to Ti.

The secondary healing conditions *via* mechanical stimulus were visualized for the external callus, considering both implants as can be seen in Figure 6. The callus showed higher possibility for secondary healing when Mg implants was used.

4. Discussion

To evaluate the suitability of the Mg implants in hard tissue replacement applications, this *in silico* study has been performed. The conditions of the fracture site and loading scenarios at the initial phase after implantation has been simulated. The mechanical stimulus caused due to the interfragmentary strains were taken as the source for secondary healing. This study reflects the influence of stiffness of the implant material on the mechanical stimulus. Where, Ti-based implant took the majority of load when induced at the fractured part, this was not the case when the based material was replaced with Mg. In the simulation of the gait cycle, where Mg led to a higher stress concentration in the range of 0–20 MPa than that of Ti, Ti had an upper hand for the higher stress concentration range. Moreover, the maximum von Mises stress in Ti implant was found out to be 177 MPa as compared to 145 MPa in Mg implant. This stress level can be considered safe for Mg implants as it is lower than the yield stress of extruded Mg alloys and even partly lower than that of the alloyed and extruded Mg (Wiese et al. 2021, 2022) The *stress shielding* problem is highly associated with the rigidity of the metallic implants such as Ti, given to their high *E* value (108 GPa) for a given geometry. This was also seen in the simulation results. Due to high *E* value, Ti has considerably lower strain than that of Mg for the same amount of stress, thus for the majority of the loading conditions, bone does not experience any load. This was also seen when the stress conditions at the screws for both implants were compared. The screws share the load between the fractured bone and the implant (Mehboob et al. 2020). For generating appropriate IFM at the fracture site, the stress on the screws should also be modulated. The Ti screws carried slightly higher stress than that of Mg screws. This led to minimal strain at the fracture site for Ti implants. This was seen, when the hydrostatic and octahedral shear strain distribution of the central
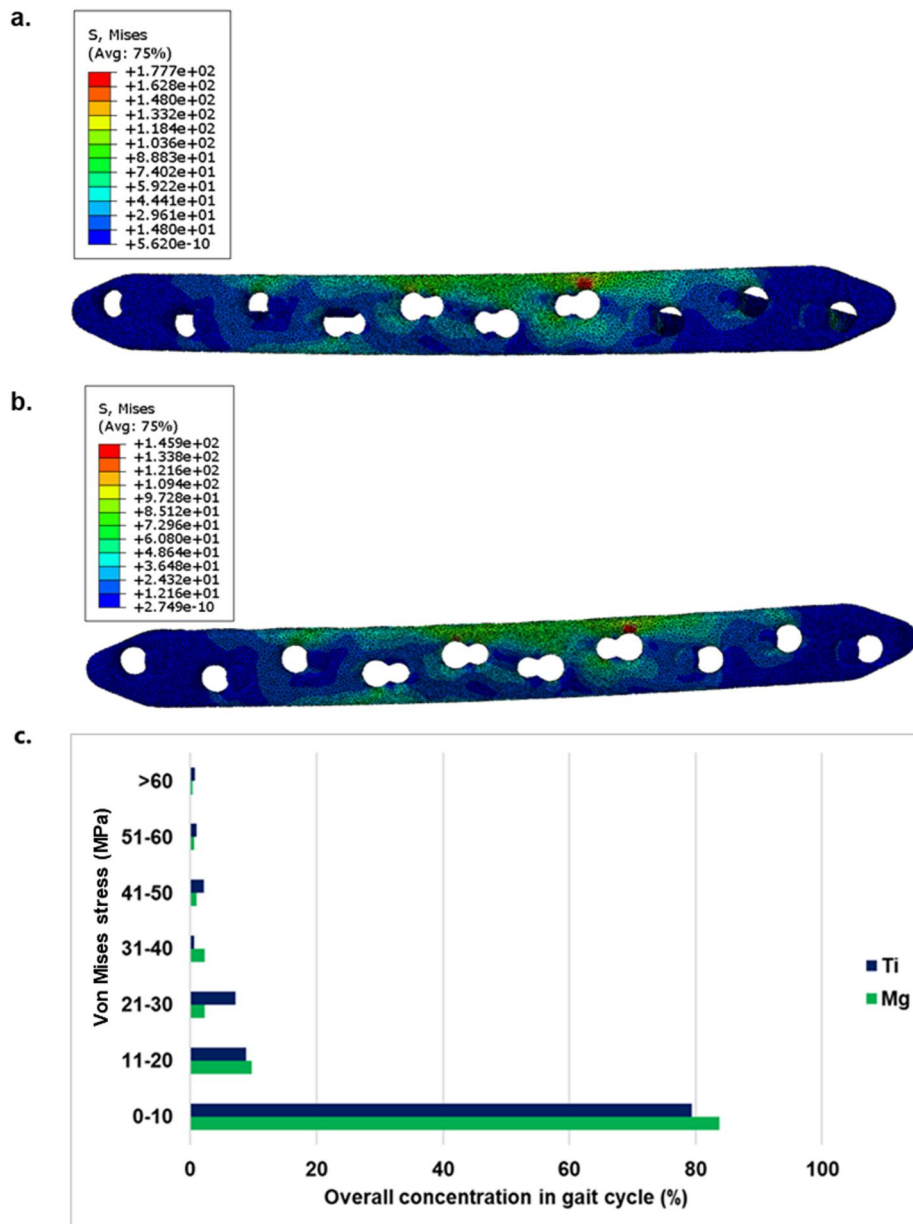
Figure 3. The von mises stress distribution in MPa for a. Ti and b. Mg implant at the same stage of a gait cycle; c. The overall stress distribution for Mg and Ti implants in a gait cycle. More stress was taken by Ti as compared to Mg.

callus was compared for both implant scenarios. The interfragmentary strains at the central callus was slightly higher for Mg implants than that of Ti. This had positive influence in the overall mechanical stimulus for the external callus. Even though, the external callus had a slightly higher ratio of 'too much' stimulus in Mg implant case, the overall ratio for perfect mechanical stimulus was found to be higher in this case, whereas callus had slightly higher 'lazy' stimulus for Ti implants. The E of Mg (45 GPa) is significantly closer to bone ($\sim$20 GPa) (Cuppone et al. 2004) than that of Ti, thus it can act as a proper support for the bone where a better mechanical stimulus for bone healing can be achieved. This was also verified in other

previous studies (Sha et al. 2009; Kim et al. 2011; Bigham-Sadegh and Oryan 2015; Mehboob and Chang,2018 2019). Nails made of two Ti alloys were investigated, one with a high-rigidity (Ti-6Al-4V with 110 GPa) and one with a low-rigidity (Ti-24Nb-4Zr-7.9Sn with 33 GPa). In this study, the influence of the lower rigidity on better external callus formation and a reduced bone resorption than the high-rigidity nail was determined. Mg alloys have a similarly lower E value along with the possibility of contributing an additional beneficial biological effect on fracture healing (Burmester et al. 2017; Zhou et al. 2021).

The results found at the external callus also support the previous experimental study, where Mg nails
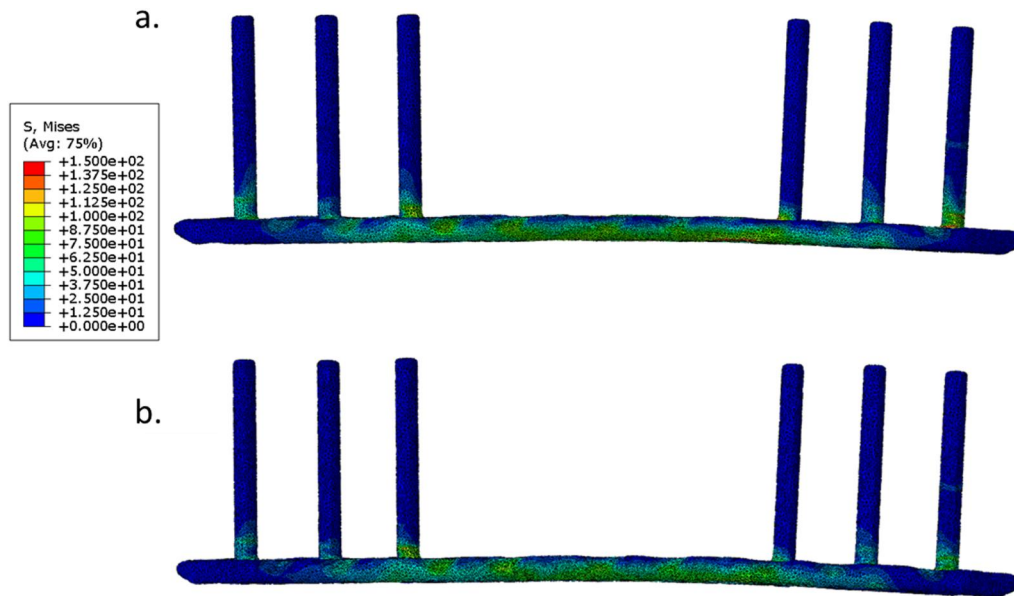
Figure 4. Stress overview at the screw location for a. Ti implant, b. Mg implant at the same stage of a gait cycle. Slightly higher stress levels were found for ti than that of Mg.
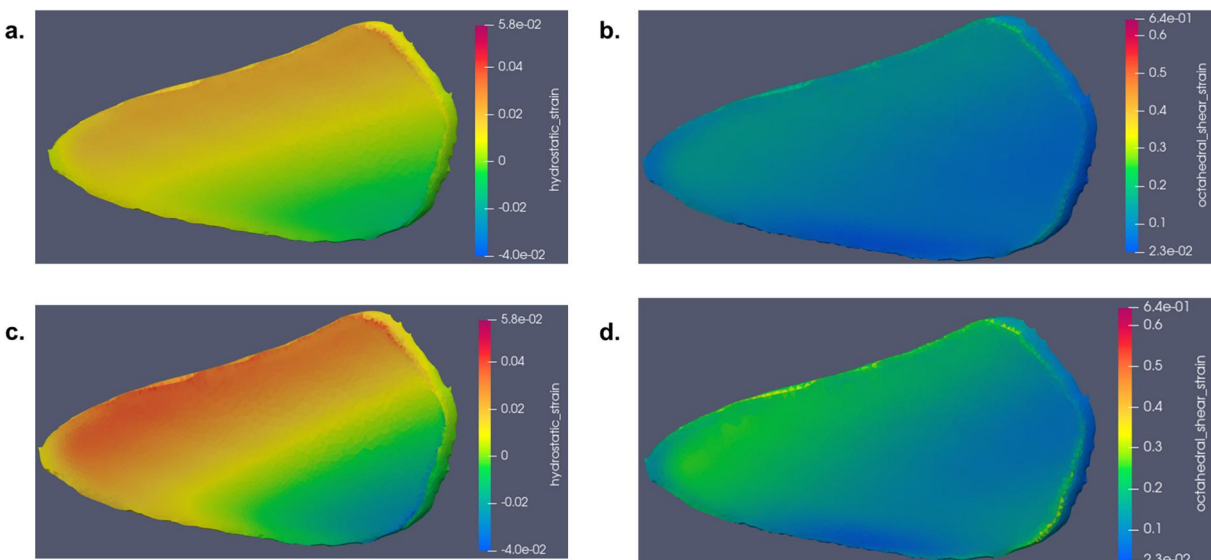
Figure 5. Hydrostatic strain and octahedral strain distribution in the fracture callus in the same stage of a gait cycle for (a, b) Ti implant and (c, d) Mg implant. Higher strain values were found when Mg implant was used.

augmented the callus formation in *in vivo* studies (Jähn et al. 2016). The influence of the mechanical properties of the implant on the callus growth was clearly seen in the results. As Ti absorbed major part of the mechanical stress, the callus did not have the higher chance of secondary healing which was not the case for Mg implants. Similar results were also found by Fouda et al. (2019) in the simulation study where SLS and Carbon/hydroxyapatite (C/HA) were compared for better fracture healing of tibia. In that study, lower stress shielding of C/HA was given to be the major factor behind better secondary healing than SLS implant. The Mg implants also have advantage in

terms of its biodegradability that along with favouring the superior bone healing conditions also limit the need for implant removal operation.

Nonetheless, the results in this study only corresponds to the initial phase after implantation. The influence of Mg degradation in long term study has not been performed in this study. However, the results resonate with the study performed by Mehboob et al. (2020) where a 30-day healing simulation was compared for biodegradable Mg based composites and SLS bone plates. The study proposed that the decaying stiffness of degradable implant reduced the *stress shielding* effects, which led to an
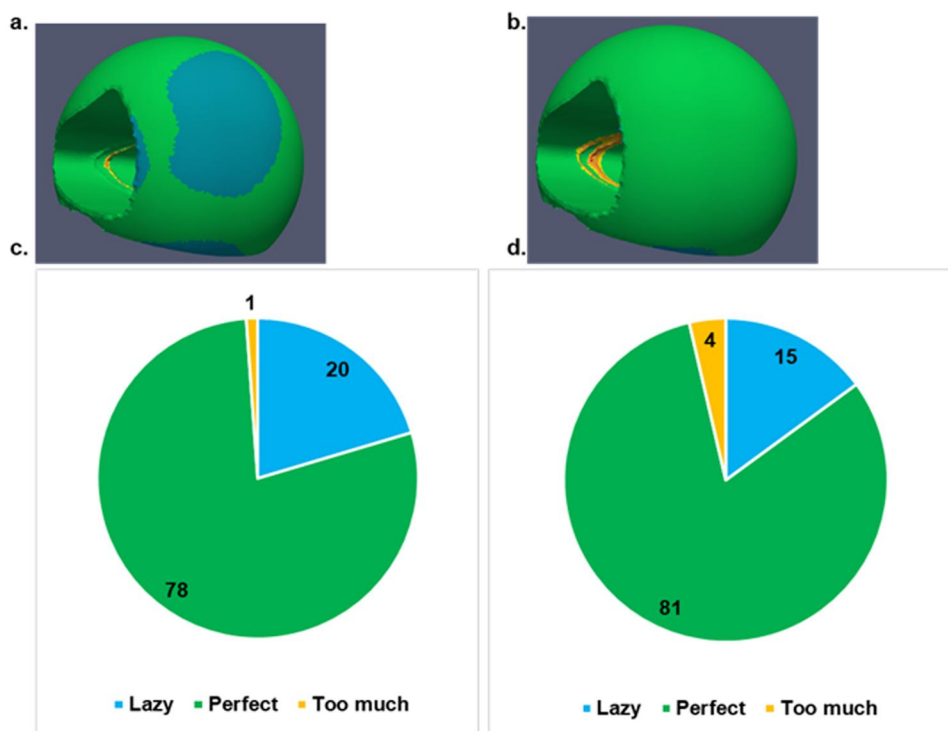
Figure 6. The mechanical stimulus distribution in the external callus at the same stage of a gait cycle for a. Ti and b. Mg implant; the overall mechanical stimulus distribution percentage in callus for c. Ti, and d. Mg implant in a gait cycle. The better mechanical stimulus for bone development was found when Mg was used as implant.

improvement in biomechanical stimulus. Due to this reason, the Mg based composites showed better healing than that of SLS bone plates.

However, to have a better correlation between Mg degradation and new bone formation throughout the bone remodeling phase, the influence of degradation in biology and mechanics is also need in the current model. This can help in understanding the best possible condition needed for the implant to degrade with minimal negative influence on bone reformation.

5. Conclusions

In this study, the initial phase of bone healing at tibia fracture site was simulated. The influence of the implant material on stimulus required for development of callus into bone was investigated, where Mg was compared with Ti. The loading conditions in tibia during gait cycle were used as input. The lower stiffness of Mg implant helped in providing better mechanical stimulus for bone formation in callus. As Ti implant took major amount of load, the callus was seen to have little lower stimulus which can delay healing. This was also confirmed by the von Mises stress distribution in these two implants during the gait cycle. Moreover, the more even load distribution

in the implant reduces the maximum stress in the implant. In this case, this low stress allows Ti-based implants to be replaced 1-to-1 by Mg-based implants.

However, as Mg is a biodegradable implant, this study only confirms the initial phase of bone healing. In the next phase of this study, the biodegradability of the Mg will be coupled in this model to provide a better overview about the possibility of applying Mg implant to repair tibia fracture in a long term.

Disclosure statement

No potential conflict of interest was reported by the author(s).

Funding

This research received no external funding.

Data availability statement

The data presented in this study could be obtained on request from the corresponding author.

Conflicts of interest

The authors declare no conflict of interest.

References

Acar B, Kose O, Unal M, Turan A, Kati YA, Guler F. 2020. Comparison of magnesium versus titanium screw fixation for biplane chevron medial malleolar osteotomy in the treatment of osteochondral lesions of the talus. Eur J Orthop Surg Traumatol. 30(1):163–173. doi: 10.1007/s00590-019-02524-1.

Bergmann G, Bender A, Graichen F, Dymke J, Rohlmann A, Trepczynski A, Heller MO, Kutzner I. 2014. Standardized loads acting in knee implants. PLoS One. 9(1):e86035. doi: 10.1371/journal.pone.0086035.

Bigham-Sadegh A, Oryan A. 2015. Basic concepts regarding fracture healing and the current options and future directions in managing bone fractures. Int Wound J. 12(3):238–247. doi: 10.1111/iwj.12231.

Braun BJ, Orth M, Diebels S, Wickert K, Andres A, Gawlitza J, Bücker A, Pohlemann T, Roland M. 2021. Individualized determination of the mechanical fracture environment after tibial exchange nailing: a simulation-based feasibility study. Front Surg. 8:749209. doi: 10.3389/fsurg.2021.749209.

Burmester A, Willumeit-Römer R, Feyerabend F. 2017. Behavior of bone cells in contact with magnesium implant material. J Biomed Mater Res B Appl Biomater. 105(1):165–179. doi: 10.1002/jbm.b.33542.

Claes LE, Heigele CA. 1999. Magnitudes of local stress and strain along bony surfaces predict the course and type of fracture healing.

Cuppone M, Seedhom BB, Berry E, Ostell AE. 2004. The longitudinal Young's modulus of cortical bone in the midshaft of human femur and its correlation with CT scanning data. Calcif Tissue Int. 74(3):302–309. doi: 10.1007/s00223-002-2123-1.

De Fátima Ferreira Mariotto S, Guido V, Cho LY, Soares CP, Cardoso KR. 2011. Porous stainless steel for biomedical applications. Mater Res. 14(2):146–154. doi: 10.1590/S1516-14392011005000021.

Farabi E, Sharp J, Vahid A, Wang J, Fabijanic DM, Barnett MR, Corujeira Gallo S. 2021. Novel biodegradable Zn alloy with exceptional mechanical and in vitro corrosion properties for biomedical applications. ACS Biomater Sci Eng. 7(12):5555–5572. doi: 10.1021/acsbiomaterials.1c00763.

Fouda N, Mostafa R, Saker A. 2019. Numerical study of stress shielding reduction at fractured bone using metallic and composite bone-plate models. Ain Shams Eng J. 10(3):481–488. doi: 10.1016/j.asej.2018.12.005.

Ganadhiepan G, Miramini S, Mendis P, Patel M, Zhang L. 2021. A probabilistic approach for modelling bone fracture healing under Ilizarov circular fixator. Numer Methods Biomed Eng. 37(7):1–20. doi: 10.1002/cnm.3466.

Goharian A, Abdullah MR. 2017. Bioinert metals (stainless steel, titanium, cobalt chromium). Amsterdam: Elsevier. doi: 10.1016/b978-0-12-804634-0.00007-0.

Han P, Cheng P, Zhang S, Zhao C, Ni J, Zhang Y, Zhong W, Hou P, Zhang X, Zheng Y, et al. 2015. *In vitro* and *in vivo* studies on the degradation of high-purity Mg (99.99wt.%) screw with femoral intracondylar fractured rabbit model. Biomaterials. 64:57–69. doi: 10.1201/b18932.

Imam MA, Fraker AC. 1996. Titanium alloys as implant materials. Medical applications of titanium and its alloys: the material and biological issues. ASTM Int. 3–16. doi: 10.1520/stp16066s.

Jähn K, Saito H, Taipaleenmäki H, Gasser A, Hort N, Feyerabend F, Schlüter H, Rueger JM, Lehmann W, Willumeit-Römer R, et al. 2016. Intramedullary Mg_2Ag nails augment callus formation during fracture healing in mice. Acta Biomater. 36:350–360. doi: 10.1016/j.actbio.2016.03.041.

Kim HJ, Kim SH, Chang SH. 2011. Finite element analysis using interfragmentary strain theory for the fracture healing process to which composite bone plates are applied. Compos Struct. 93(11):2953–2962. doi: 10.1016/j.compstruct.2011.05.008.

Lacroix D, Prendergast IPJ, Li IG, Marsh D. 2002. Biomechanical model to simulate tissue differentiation and bone regeneration: application to fracture healing. Med Biol Eng Comput. 40(1):14–21. doi: 10.1007/BF02347690.

Li N, Zheng Y. 2013. Novel magnesium alloys developed for biomedical application: a review. J Mater Sci Technol. 29(6):489–502. doi: 10.1016/j.jmst.2013.02.005.

López HY, Cortés-Hernández DA, Escobedo S, Mantovani D. 2006. *In vitro* bioactivity assessment of metallic magnesium. KEM. 309–311:453–456. doi: 10.4028/www.scientific.net/KEM.309-311.453.

Lu Y, Lekszycki T. 2017. Modelling of bone fracture healing: influence of gap size and angiogenesis into bioresorbable bone substitute. Math Mech Solids. 22(10):1997–2010. doi: 10.1177/1081286516653272.

McCracken M. 1999. Dental implant materials: commercially pure titanium and titanium alloys. J Prosthodont. 8(1):40–43. doi: 10.1111/j.1532-849X.1999.tb00006.x.

Mehboob A, Chang SH. 2018. Biomechanical simulation of healing process of fractured femoral shaft applied by composite intramedullary nails according to fracture configuration. Compos Struct. 185:81–93. doi: 10.1016/j.compstruct.2017.11.002.

Mehboob A, Chang SH. 2018. Effect of composite bone plates on callus generation and healing of fractured tibia with different screw configurations. Compos Sci Technol. 167:96–105. doi: 10.1016/j.compscitech.2018.07.039.

Mehboob A, Chang SH. 2019. Effect of initial micro-movement of a fracture gap fastened by composite prosthesis on bone healing. Compos Struct. 226:111213. doi: 10.1016/j.compstruct.2019.111213.

Mehboob A, Rizvi SHA, Chang SH, Mehboob H. 2020. Comparative study of healing fractured tibia assembled with various composite bone plates. Compos Sci Technol. 197:108248. doi: 10.1016/j.compscitech.2020.108248.

Mehboob H, Chang SH. 2014. Application of composites to orthopedic prostheses for effective bone healing: a review. Compos Struct. 118:328–341. doi: 10.1016/j.compstruct.2014.07.052.

Miramini S, Zhang L, Richardson M, Mendis P, Ebeling PR. 2016. Influence of fracture geometry on bone healing under locking plate fixations: a comparison between oblique and transverse tibial fractures. Med Eng Phys. 38(10):1100–1108. doi: 10.1016/j.medengphy.2016.07.007.

Orth M, Ganse B, Andres A, Wickert K, Warmerdam E, Müller M, Diebels S, Roland M, Pohlemann T. 2023. Simulation-based prediction of bone healing and treatment recommendations for lower leg fractures: effects of motion, weight-bearing and fibular mechanics. Front Bioeng Biotechnol. 11:1067845. doi: 10.3389/fbioe.2023.1067845.

Rack HJ, Qazi JI. 2006. Titanium alloys for biomedical applications. Mater Sci Eng C. 26(8):1269–1277. doi: 10.1016/j.msec.2005.08.032.

Razavi M, Fathi MH, Meratian M. 2010. Fabrication and characterization of magnesium–fluorapatite nanocomposite for biomedical applications. Mater Char. 61(12):1363–1370. doi: 10.1016/j.matchar.2010.09.008.

Rho JY, Hobatho MC, Ashman RB. 1995. Relations of mechanical properties to density and CT numbers in human bone. Med Eng Phys. 17(5):347–355. doi: 10.1016/1350-4533(95)97314-f.

Ridzwan MIZ, Shuib S, Hassan AY, Shokri AA, Mohamad Ib MN. 2007. Problem of stress shielding and improvement to the hip implant designs: a review. J Med Sci. 7(3):460–467. doi: 10.3923/jms.2007.460.467.

Schwarzenberg P, Ren T, Klein K, von Rechenberg B, Darwiche S, Dailey HL. 2021. Domain-independent simulation of physiologically relevant callus shape in mechanoregulated models of fracture healing. J Biomech. 118:110300. doi: 10.1016/j.jbiomech.2021.110300.

Sha M, Guo Z, Fu J, Li J, Yuan CF, Shi L, Li SJ. 2009. The effects of nail rigidity on fracture healing in rats with osteoporosis. Acta Orthop. 80(1):135–138. doi: 10.1080/17453670902807490.

Shefelbine SJ, Augat P, Claes L, Simon U. 2005. Trabecular bone fracture healing simulation with finite element analysis and fuzzy logic. J Biomech. 38(12):2440–2450. doi: 10.1016/j.jbiomech.2004.10.019.

Sorriento A, Chiurazzi M, Fabbri L, Scaglione M, Dario P, Ciuti G. 2021. A novel capacitive measurement device for longitudinal monitoring of bone fracture healing. Sensors. 21(19):6694. doi: 10.3390/s21196694.

Steiner M, Claes L, Ignatius A, Niemeyer F, Simon U, Wehner T. 2013. Prediction of fracture healing under axial loading, shear loading and bending is possible using distortional and dilatational strains as determining mechanical stimuli. J R Soc Interface. 10(86):20130389. doi: 10.1098/rsif.2013.0389.

Weinans H, Huiskes R, Grootenboert HJ. 1992. The behavior of adaptive bone-remodeling simulation models.

Wiese B, Harmuth J, Willumeit-Römer R, Bohlen J. 2022. Property variation of extruded Mg–Gd alloys by Mn addition and processing. Crystals (Basel). 12(8):1036. doi: 10.3390/cryst12081036.

Wiese B, Willumeit-Römer R, Letzig D, Bohlen J. 2021. Alloying effect of silver in magnesium on the development of microstructure and mechanical properties by indirect extrusion. J Magnes Alloys. 9(1):112–122. doi: 10.1016/j.jma.2020.08.001.

Zeng Z, Salehi M, Kopp A, Xu S, Esmaily M, Birbilis N. 2022. Recent progress and perspectives in additive manufacturing of magnesium alloys. J Magnes Alloys. 10(6):1511–1541. doi: 10.1016/j.jma.2022.03.001.

Zhou H, Liang B, Jiang H, Deng Z, Yu K. 2021. Magnesium-based biomaterials as emerging agents for bone repair and regeneration: from mechanism to application. J Magnes Alloys. 9(3):779–804. doi: 10.1016/j.jma.2021.03.004.